Journal of GeoEngineering, Vol. 14, No. 2, pp. 77-84, June 2019
http://dx.doi.org/10.6310/jog.201906_14(2).3

GROUND-MOTION SIMULATIONS OF A LISTRIC NORMAL FAULT FOR PROBABILISTIC SEISMIC HAZARD ANALYSIS

Yin-Tung Yen [1*], Ming-Che Hsieh [2], Po-Shen Lin [3], and Pao-Shan Hsieh [4]

ABSTRACT

In general, in probabilistic seismic hazard analysis, the ground motion prediction equation (GMPE) is suitable for evaluating ground motions from fault sources with a single dipping angle. However, for the complex fault rupture cases of listric faults that have two or more dipping angles, it is difficult to use the GMPE for seismic hazard analysis because of the nature of its functional form. The overall characteristics of ground motion at a specific site of interest need to be determined through multiple earthquake scenarios *via* ground motion simulations. Therefore, it is necessary to compare ground motions from GMPE prediction and simulated data in order to set the GMPE for use in seismic hazard analysis. In this study, we employ a ground-motion simulation to evaluate GMPE input parameters for listric normal fault cases. We show that quantitatively comparing ground motions from GMPE prediction and simulated data is a feasible method for defining input parameters for the GMPE in seismic hazard analysis.

Key words: Ground motion simulation, listric normal fault, ground motion prediction equation, probabilistic seismic hazard analysis.

1. INTRODUCTION

Probabilistic seismic hazard analysis (PSHA) is currently utilized to develop design specifications for different levels of ground motion (*e.g.*, design spectrum and peak ground acceleration) and to capture the seismic hazard level for a specific site (Cheng *et al*. 2007). Figure 1 shows a simplified flowchart of the PSHA scheme. To implement PSHA, the first step is to characterize the seismic sources, including active faults, area sources, and subduction sources. Then, the earthquake recurrence rate of each seismic source is evaluated from the exponential or characteristic models. Once the seismic sources and their related recurrence rates are identified, we can use a ground motion model — or more specifically, the ground motion prediction equation (GMPE) — to express the ground motion level from the seismic sources at the site and estimate the probability of exceedance of ground motion level.

Due to the robustness and reliability of GMPE models as well as their ease of implementation, as shown by the ground motion framework in Fig. 1, GMPEs are still a standard tool for ground motion prediction in hazard analyses (Douglas *et al*. 2016). The prediction of ground motion is a key component for the final hazard level. Thus, reducing uncertainties from ground motion prediction by selecting proper GMPEs for PSHA is a critical issue.

Due to the nature of its functional form, most GMPEs are only suitable for evaluating ground motions from rectangular fault geometries with single dipping angles. For the complex fault rupture cases of listric normal faults that have at least two dipping angles, the proper value of the dipping angle needs to be evaluated for GMPE input. In this study, we examine applications of ground motion simulation to explore the applicability of GMPEs for listric normal faulting.

2. THE EXSIM GROUND MOTION SIMULATION METHOD

In this study, we used EXSIM for ground motion simulation. EXSIM is a stochastic finite-fault simulation algorithm (Atkinson and Assatourians 2015) for producing the acceleration time histories of earthquakes. In EXSIM, a fault plane is defined, with a specified size according to its seismic moment, and divided into a matrix of subsources, each of which is treated as a point source. Acceleration time series from the subsources are modeled using the point-source stochastic model. The ground motion from each subsource is treated as random Gaussian noise of a specified duration, with an underlying spectrum as given by the Brune point-source model for shear radiation (Brune 1970; Brune 1971). The Brune model specifies the Fourier spectrum at the source by a seismic moment and stress parameter and is attenuated in the frequency domain according to an empirical attenuation model. The time series from the subsources are summed in the time domain, with appropriate time delays according to the propagation of the rupture front. EXSIM is a representative stochastic ground motion simulation method, and it has been verified by the Southern California Earthquake Center (SCEC) and validated by crustal and subduction-zone earthquakes (Goulet *et al*. 2014).

Rupture models for a given fault geometry are generated by a number of random slip distributions, and each of them is the result of an individual simulation. In EXSIM simulations, a listric fault case can be revealed by a situation with two dipping angles for two rupture models. If regional differences are considered,

Manuscript received February 27, 2018; revised October 16, 2018; accepted October 19, 2018.
[1*] Researcher (corresponding author), Sinotech Engineering Consultants, Inc., Taipei, Taiwan 114, R.O.C. (e-mail: ytyen@sinotech.org.tw).
[2] Associate Researcher, Sinotech Engineering Consultants, Inc., Taipei, Taiwan 114, R.O.C.
[3] Researcher, Sinotech Engineering Consultants, Inc., Taipei, Taiwan 114, R.O.C.
[4] Associate Researcher, Sinotech Engineering Consultants, Inc., Taipei, Taiwan 114, R.O.C.

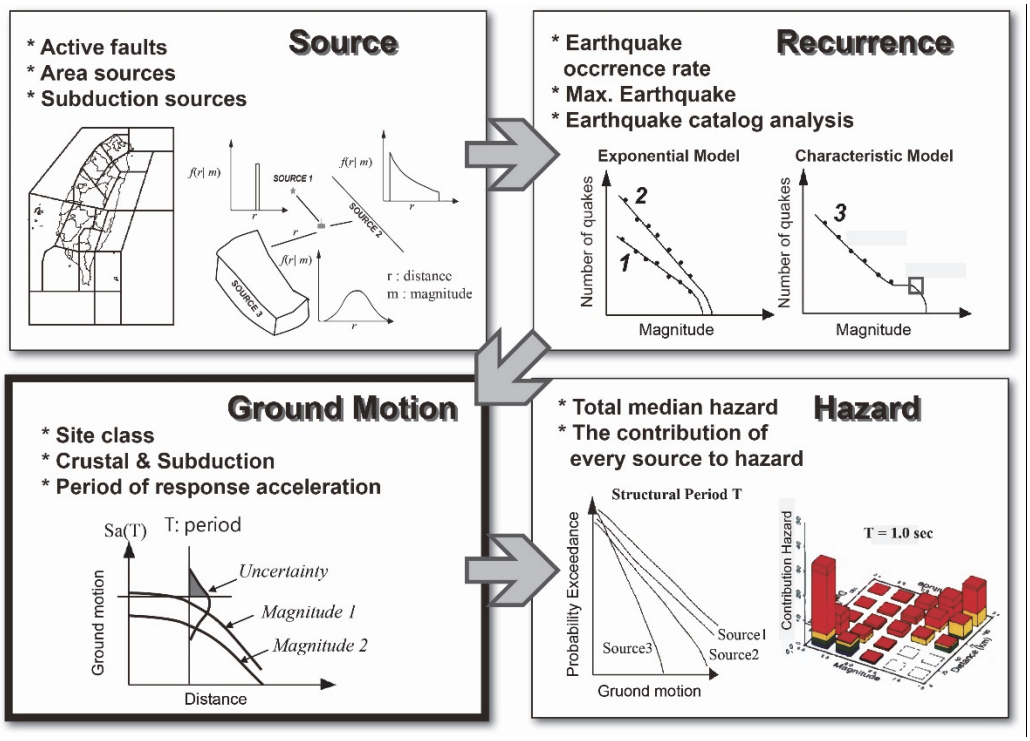

Fig. 1 Flowchart of probabilistic seismic hazard analysis

a stochastic model of the region of interest for ground motion simulation should be developed. Although common parameters need to be set for EXSIM simulations, in this study, we do not adjust them for regional differences. Instead, we focus on the dipping angle parameters. Thus, we take the ratio of ground levels (*i.e.*, response spectra) for a listric fault case with two dipping angles and a reference case with one dipping angle. The response spectral ratio for a range of periods can be used as a basis for adjusting GMPE input parameters.

3. APPLICABILITY OF THE GMPE TO LISTRIC NORMAL FAULTS

Based on a geological survey, well logging, and seismic profiles, the fault geometries of the Shanchiao Fault structure in northern Taiwan were delineated and found to be a listric faulting system with two dipping angles. Therefore, several combinations of dipping angles and fault widths are recommended for ground motion prediction with respect to the uncertainty of seismogenic depth in northern Taiwan. We focused on the hazard contribution of the major faults in the study sites. According to the prescribed fault geometry, the target sites are located on a hanging wall. Henceforth, we carefully evaluated the ground motion of the listric normal fault at a site 5 km away from the fault source for the use of GMPEs in seismic hazard analysis.

We selected the upper segment of the Shanchiao Fault with its dipping angle as a reference case (shown in Fig. 2 as "Ref. case"), and a two-dipping-angle fault model was proposed as a control case. We used the scaling relationship derived from the reference and control cases to determine whether the GMPE was capable of calculating reasonable ground motions from listric normal faults. In Fig. 2, the control cases of A1, A2, and A3 are, respectively, fault models with (1) a dipping angle from the upper segment, (2) a dipping angle from the lower segment, and (3) a dipping angle averaged from the upper and lower segments for application in the GMPEs. We took each individual case as an approach for the GMPE. Therefore, approaches 1, 2, and 3 were for cases A1, A2, and A3, respectively. Furthermore, the Southwestern United States Project for the Diablo Canyon Nuclear Power Plant used the SRSS (*i.e.*, the square root of the sum of the response spectrum squares) (GeoPantech 2015), and the resulting response spectra from the upper and lower portions were used to compute a single response spectrum (Case D). The SRSS computes the square root of the sum of the response spectrum squares from each of the individual rupture segments. The ground motion can be considered to be the combination of the ground motions from separate sub-faults from a depth extended rupture.

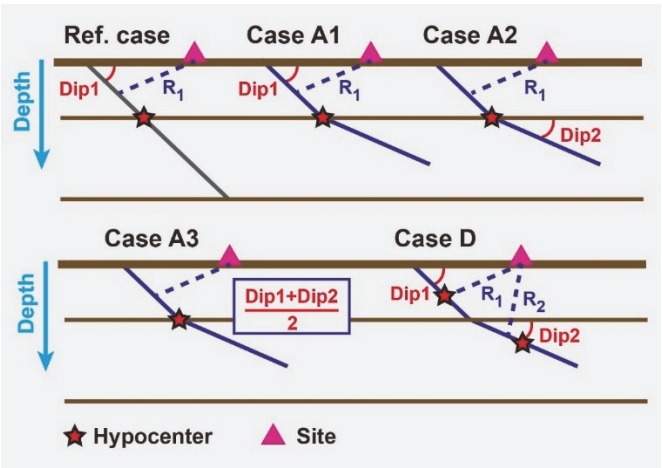

Fig. 2 Schematic diagram of listric normal fault models. R_1 and R_2 are the closest distances from the station to the fault plane

We calculated the response spectra for the four approaches and a single dipping angle for the upper segment (*i.e.*, the reference case) by using GMPEs, as shown in Fig. 3(a). We conducted a total of thirty ground motion simulations for each case using fault models with (1) two dipping angles for the upper and lower segments and (2) a single dipping angle for the upper segment. Then, an averaged response spectrum was calculated from the thirty simulations (*i.e.*, thirty random distributions in the EXSIM simulations), as shown in Fig 3(b). The scaling relationship was determined by calculating the spectral ratios of the two-dipping-angle and single-dipping-angle cases (*i.e.*, simulation/simulation_Ref) for the simulations and the GMPE calculation results for each approach (*i.e.*, GMPE(Approach)/GMPE_Ref.). We expect the spectral ratio of the two-dipping-angle and single-dipping-angle cases from the EXSIM simulations to be the correct one. We used the spectral ratio from simulations as a criterion for evaluating the best GMPE approach, as shown in Fig 3(c). For the calculation of the response spectrum, we used approaches 1, 2, and 3 and the SRSS approach for cases A1, A2, A3, and D, respectively. Thus, we compared the spectral ratios from the four approaches with the simulated spectra to determine appropriate values for the dipping angle of the listric normal fault input to the GMPEs.

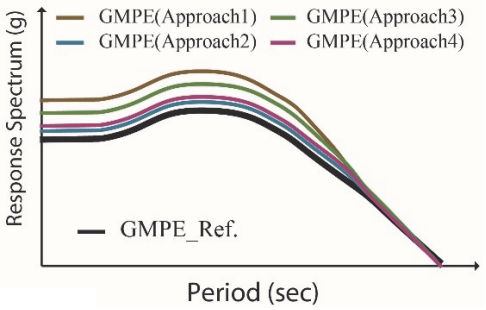

(a) The original response spectra of the listric fault case and ref. case

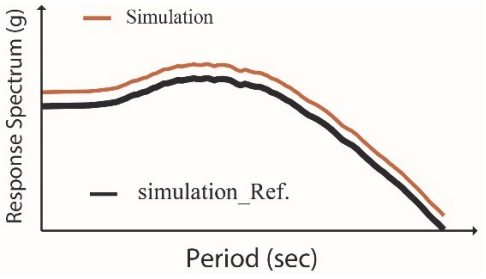

(b) The original response spectra of the listric fault case and ref. case

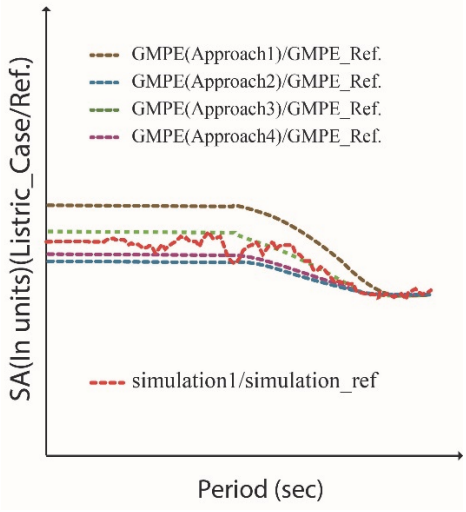

(c) A comparison of the results

Fig. 3 Schematic diagram of developing a comparison between the simulated and GMPE-predicted ratios of mean response spectra

Figure 4 shows a schematic plot of listric normal fault cases that can be practically implemented in simulation analyses. Note: The triangles represent fictitious stations and the two dashed lines are the closest paths from the station to the fault plane. The distances to the upper and lower segments for M(60, 25, *km) and M(70, 25, *km) are (4.3 km, 6.2 km) and (4.7 km, 9.2 km), respectively. *km means a various parameter that we will set 10, 15, and 20 km. Gray lines are reference cases with one dipping angle. Red and blue lines are, respectively, the upper and lower segments of the listric normal fault model. From the viewpoint of geology and tectonic settings, the dip of the Shanchiao Fault and the seismogenic depth in the adjacent region are still under debate. The seismogenic depth is the depth at which the isostasy of the top of the upper crust is ruptured. In general, a fault rupture extends down to the seismogenic depth. We determined the potential range in order to evaluate the effect. Two dipping angles of 60° and 70° for the upper segment and a single dipping angle of 25° for the lower segment were proposed. Furthermore, we used three seismogenic depths of 10, 15, and 20 km for ground motion simulations. Six groups — M(60, 25, 10), M(60, 25, 15), M(60, 25, 20), M(70, 25, 10), M(70, 25, 15), and M(70, 25, 20) — were studied *via* ground motion simulation and the results are displayed in Table 1; the first two variables of each bracket are the dipping angles and the third is the seismogenic depth.

As shown in Fig. 5(a), the control case of M(70, 25, 15) is defined according to the possible dipping angles of the upper and lower segments with a seismogenic depth of 15 km. It has dipping angles of 75° and 25° for the upper and lower segments, respectively. Furthermore, we designed the SIM1 and SIM2 cases to examine the differences from the location of rupture initiation. In the SIM1 case, the rupture initiated from the center of the upper segment, and we assumed a constant rupture velocity of 3.0 km/s for rupture propagation. We obtained the resulting seismogram by summation of the seismograms from the upper and lower segments with respect to a certain rupture delay time. In the SIM2 case, the only change was that the rupture initiated from the center of the lower segments. We conducted a total of thirty simulations, calculated the average response spectrum for each SIM case, and compared them. The results did not show any significant differences in rupture initiation. Spectral ratio curves of SIM1 and SIM2 are shown in Fig. 5(b).

Table 1 Magnitudes for different cases of the listric normal fault model

Seismogenic depth (km)	Ref. case (Mw)	Shallow segment (Mw)	Deep segment (Mw)
Model for a combination of 60°/25°			
10	6.78	6.54	6.68
15	7.04	6.54	7.03
20	7.21	6.54	7.22
Model for a combination of 70°/25°			
10	6.68	6.68	6.07
15	6.95	6.68	6.85
20	7.14	6.68	7.11

We selected four GMPEs, which account for fault dips in their functional forms, from the NGA-West2 Project (Bozorgnia *et al*. 2014), ASK14 (Abrahamson *et al*. 2014), BSSA14 (Boore *et al*. 2014), CB14 (Chiou and Youngs 2014), and CY14 (Campbell and Bozorgnia 2014). Comparisons of the simulation cases and the selected GMPEs are shown in Figs. 6 and 7. The results

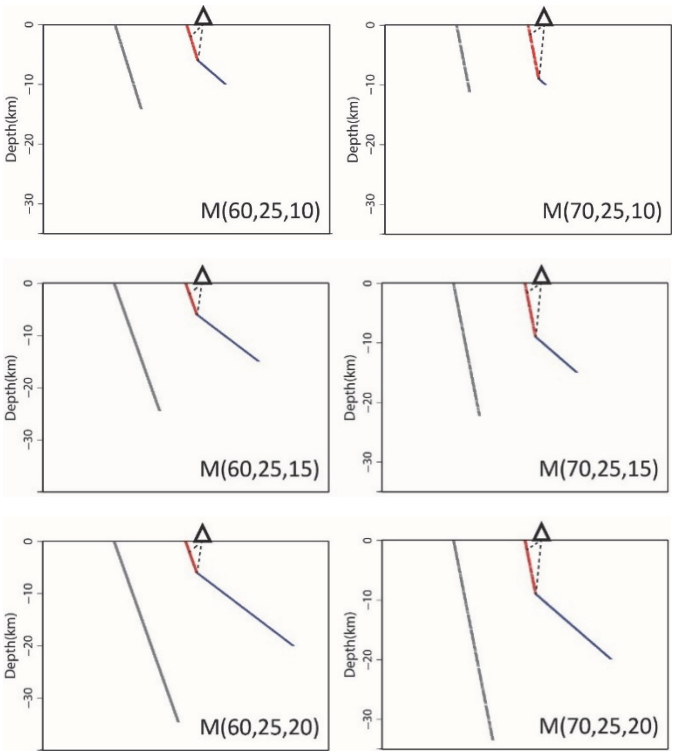

Fig. 4 Cases of listric normal faults for ground motion simulation

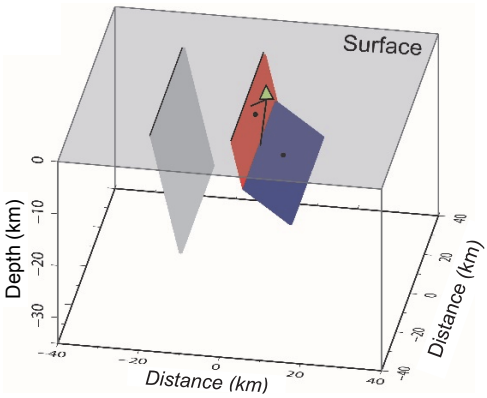

(a) A fault geometry scheme for the M(70, 25, 15) case of listric normal fault for ground motion simulation. The triangle represents the fictitious station, and gray plane expresses the reference case. The two dots indicate the hypocenters for the simulation scenarios of SIM1 and SIM2, respectively.

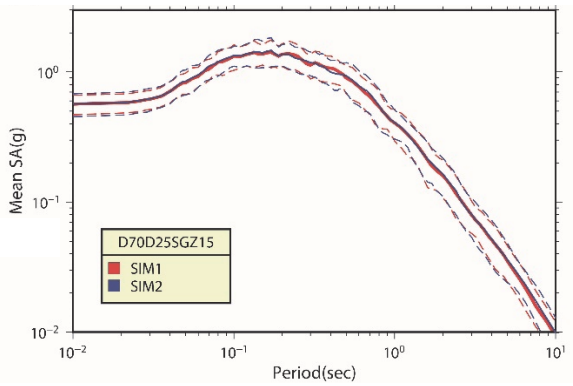

(b) Acceleration response spectra with a standard deviation from thirty simulations for SIM1 and SIM2.

Fig. 5 The scheme of fault geometry and the calculated acceleration response spectra for the simulation scenarios

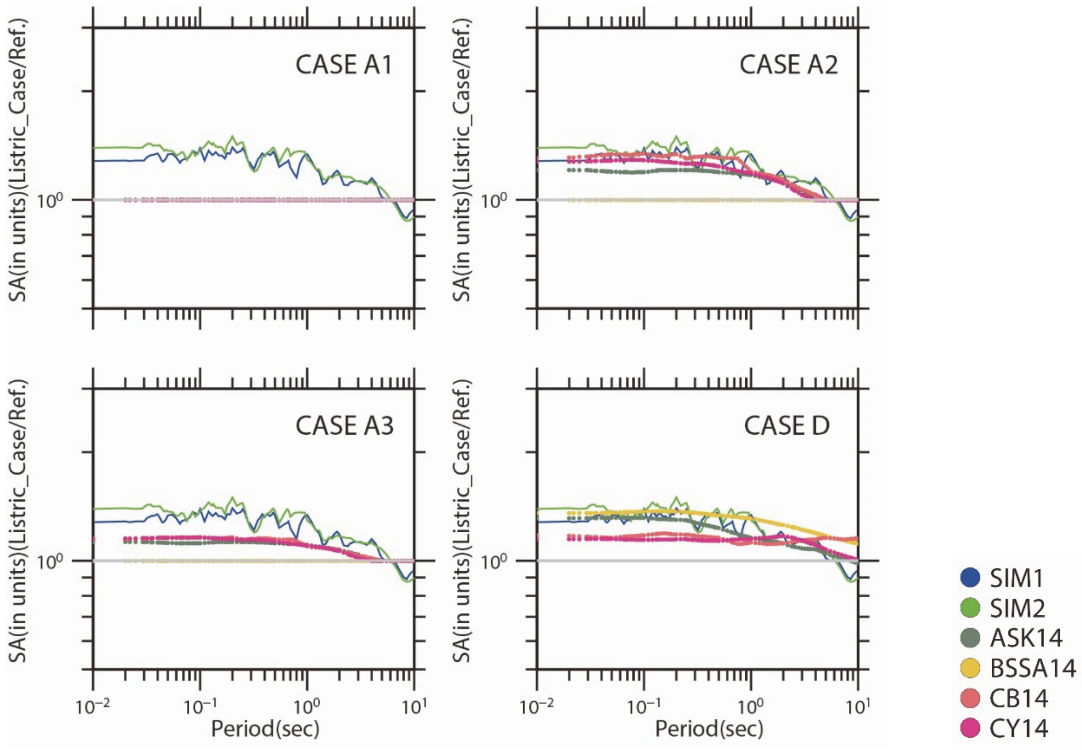

(a) M(60, 25, 10)

Fig. 6 Comparisons of simulated and GMPE-predicted response spectra

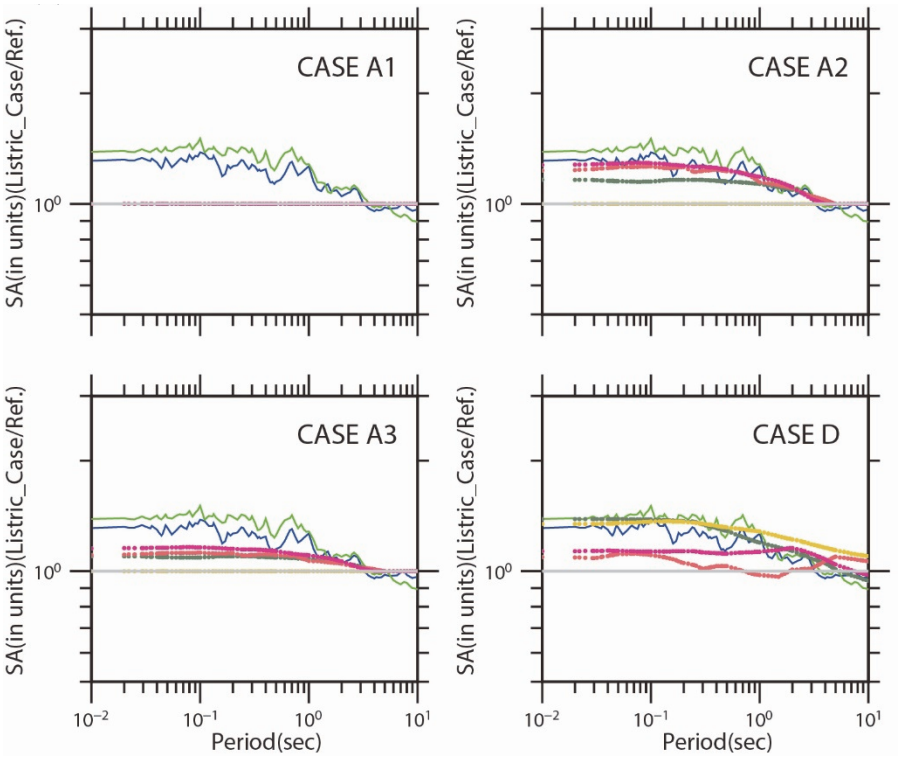

(b) M(60, 25, 15)

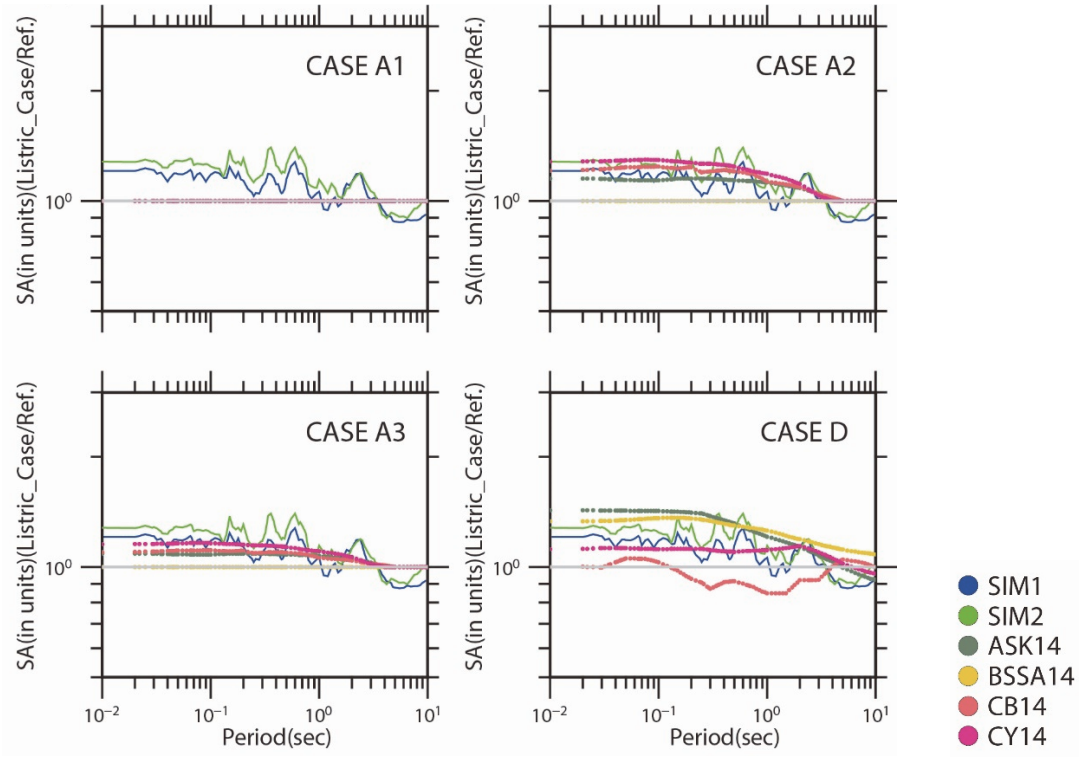

(c) M(60, 25, 20) cases

Fig. 6 Comparisons of simulated and GMPE-predicted response spectra (continued)

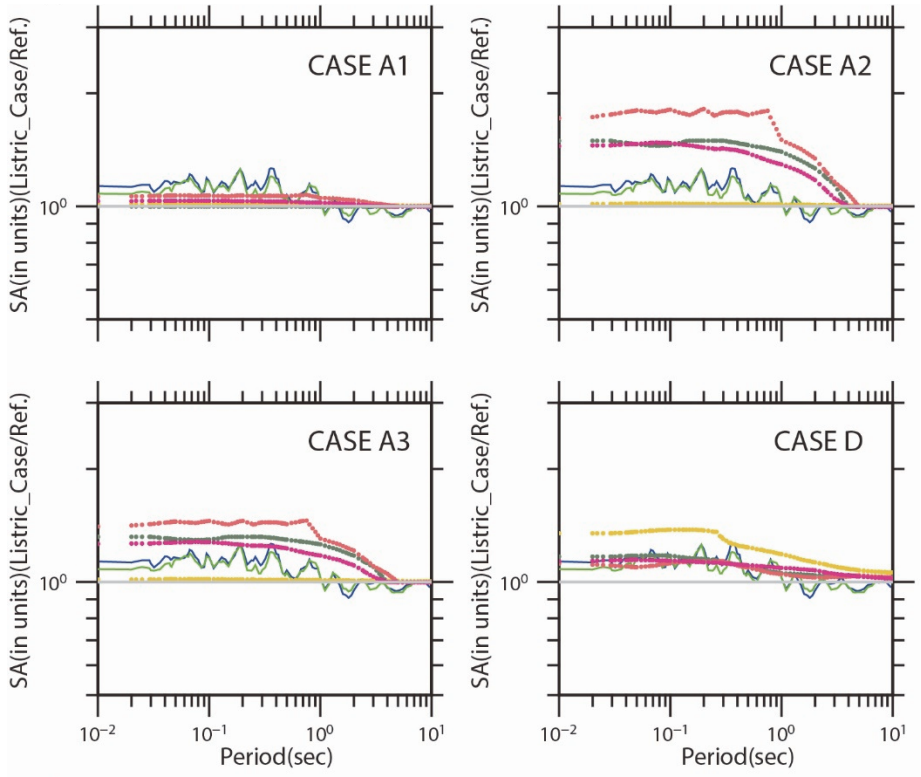

(a) M(70, 25, 10)

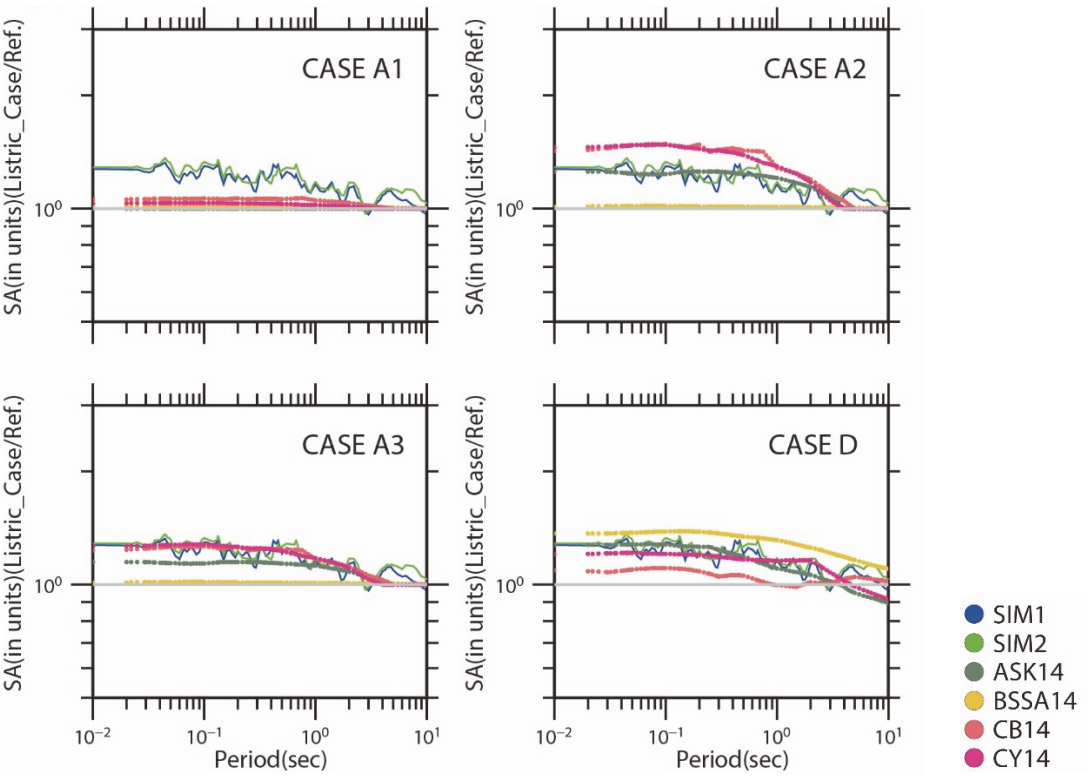

(b) M(70, 25, 15)

Fig. 7 Comparisons of simulated and GMPE-predicted response spectra

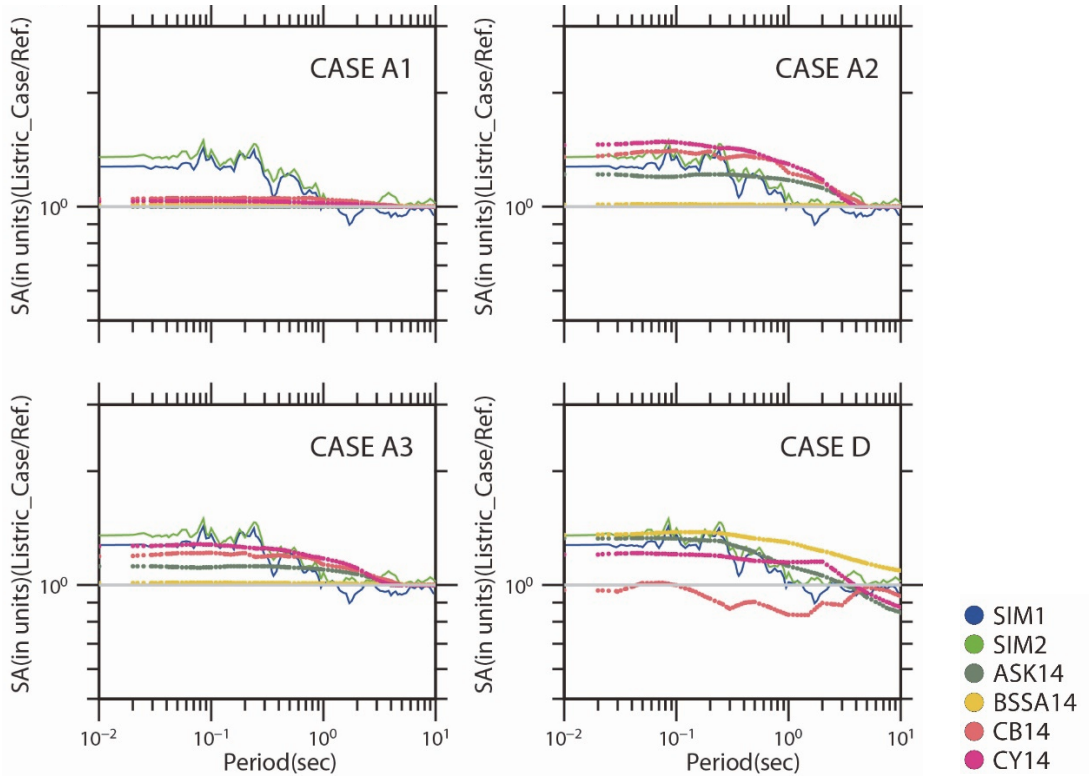

(c) M(70, 25, 20) cases

Fig. 7 Comparisons of simulated and GMPE-predicted response spectra (continued)

are categorized into two groups according to the dipping-angle pairs. In summary, for cases M(60, 25, 10), M(60, 25, 15), and M(60, 25, 20), shown in Fig. 6, for which the lower segments have larger magnitudes, the use of dips from the lower segments in the GMPEs produces a better fit (*i.e.*, Case A2). In Fig. 7, the M(70, 25, 10) case, which has a magnitude difference of greater than 0.5 between the upper and lower segments, has better agreement with GMPEs using the dip from upper segments (*i.e.*, Case A1). Furthermore, for cases M(70, 25, 15) and M(70, 25, 20), whose lower segments are larger in magnitude, the use of averaged dips from the upper and lower segments in the GMPEs produces a better fit (*i.e.*, Case A3). In addition, these comparisons show that the R_{jb}-based (Jorner-Boore distance) GMPE of BSSA14 is not suitable for the ground motion simulation of listric faults because R_{jb} is the horizontal distance to the surface projection of the rupture (*i.e.*, the Joyner-Boore distance).

4. DISCUSSION AND CONCLUSIONS

Owing to significant improvements in techniques, knowledge, experience, and computing power, physics-based ground motion simulation methods can provide the time histories, ground motion values (peak ground acceleration, velocity, and displacement), and response spectra that are necessary for engineering analyses. Ground motion prediction equations (GMPEs) remain a practical and easy-to-use tool for ground motion prediction and hazard analysis. However, too many physical parameters, such as earthquake source–slip distribution and structural heterogeneities, are omitted or simplified in most GMPE functional forms. An alternative way to balance the advantages and disadvantages of both the empirical GMPE approach and theoretical methods can contribute to achieving efficient implementation in practice.

Physics-based ground motion simulation is a powerful technique for capturing ground motion trends at a site. For example, ground motion simulation can be utilized to generate synthetic data to compensate for gaps in recorded ground motion data. However, due to lack of high-resolution data for velocity structures and site factors for correction of the ground motion simulation, we cannot precisely capture the minimum uncertainty range. Thus, we instead adopt a relative value to express a correction factor for ground motion for specific parameters in GMPEs. As an example, we implemented a ground motion simulation to determine the required input dipping angle of the fault geometry for a listric normal fault.

A summary of the findings for listric normal faults is listed below:

1. A single dipping angle for the upper segment can be used in GMPEs for listric normal fault cases when the magnitude of the upper segment is larger than the lower segment and the magnitude difference is greater than 0.5.
2. The averaged dipping angle from the upper and lower segments can be used in GMPEs for listric normal fault cases when the magnitude of the lower segment is larger than the upper segment and the magnitude difference is smaller than 0.5.
3. A single dipping angle for the lower segment can be used in GMPEs for listric normal fault cases when the magnitude of the subevent rupturing on the lower segment of the fault is larger (Mw 0.5) than the magnitude of the event on the upper segment.
4. GMPEs that are independent of dipping angle or that account for R_{jb} distance in their functional forms might not be applicable to listric normal fault cases.
5. Based on the results of the analyzed cases, for the applica-

tion of GMPEs, the distance between the site and fault trace should be approximately 5 km.

To conclude the discussions made in this study, these items are suggestions for implementing and adjusting GMPEs for the prediction of ground motions for seismic hazard analysis.

ACKNOWLEDGMENTS

The authors would like to thank the Taiwan Power Company for providing financial support and the National Center for Research on Earthquake Engineering for coordinating the SSHAC project titled "Seismic Reevaluation of Nuclear Facilities in Taiwan: Development of the Hazard Input Document for Taiwan Using SSHAC Level 3 Methodology". This study is the part of the SSHAC project.

REFERENCES

Abrahamson, N.A., Silva, W.J., and Kamai, R. (2014). "Summary of the AKS14 ground-motion relation for active crustal regions." *Earthquake Spectra*, **30**(3), 1025-1055. https://doi.org/10.1193/070913EQS198M

Atkinson, G.M. and Assatourians, K. (2015). "Implementation and validation of EXSIM (a stochastic finite-fault ground-motion simulation algorithm) on the SCEC broadband platform." *Seismological Research Letters*, **86**(1), 48-60. https://doi.org/10.1785/0220140097

Boore, D.M., Stewart, J.P., Seyhan, E., and Atkinson, G.M. (2014). "NGA-West 2 equations for predicting PGA, PGV, and 5%-damped PSA for shallow crustal earthquakes." *Earthquake Spectra*, **30**(3), 1057-1085. https://doi.org/10.1193/070113EQS184M

Bozorgnia, Y., Abrahamson, N.A., Atik, L.A., Ancheta, T.D., Atkinson, G.M., Baker, J.W., Baltay, A., Boore, D.M., Campbell, K.W., Chiou, B.S.J., Darragh, R., Day, S., Donahue, J., Graves, R.W., Gregor, N., Hanks, T., Idriss, I.M., Kamai, R., Kishida, T., Kottke, A., Mahin, S.A., Rezaeian, S., Rowshandel, B., Seyhan, E., Shahi, S., Shantz, T., Silva, W., Spudich, P., Stewart, J.P., Watson-Lamprey, J., Wooddell, K., and Youngs, R. (2014). "NGA-West 2 research project." *Earthquake Spectra*, **30**, 973-987. https://doi.org/10.1193/072113EQS209M

Brune, J. (1970). "Tectonic stress and the spectra of seismic shear waves from earthquakes." *Journal of Geophysical Research*, **75**, 4997-5009. https://doi.org/10.1029/JB075i026p04997

Brune, J. (1971). Correction to J. Brune (1970), *Journal of Geophysical Research*, **76**, 5002. https://doi.org/10.1029/JB076i020p05002

Campbell, K.W. and Bozorgnia, Y. (2014). "NGA-West2 ground motion model for the average horizontal components of PGA, PGV, and 5%-damped linear acceleration response spectra." *Earthquake Spectra*, **30**(3), 1087-1115. https://doi.org/10.1193/062913EQS175M

Cheng, C.T., Chiou, S.J., Lee, C.T., and Tsai, Y.B. (2007). "Study on probabilistic seismic hazard maps of Taiwan after Chi-Chi earthquake." *Journal of GeoEngineering*, TGS, **2**(1), 19-28. https://doi.org/10.6310/jog.2007.2(1).3

Chiou, B.S.J. and Youngs, R.R. (2014). "Update of the Chiou and Youngs NGA model for the average horizontal component of peak ground motion and response spectra." *Earthquake Spectra*, **30**(3), 1117-1153. https://doi.org/10.1193/072813EQS219M

Douglas, J. and Edwards, B. (2016). "Recent and future developments in earthquake ground motion estimation." *Earth-Science Reviews*, **160**, 203-219. https://doi.org/10.1016/j.earscirev.2016.07.005

GeoPantech (2015). *Southwestern United States Ground Motion Characterization SSHAC Level 3*, Technical Report, Rev. 2.

Goulet, C.A., Abrahamson, N.A., Somerville, P.G., and Wooddell, K.E. (2014). "The SCEC broadband platform validation exercise: Methodology for code validation in the context of seismic-hazard analyses." *Seismological Research Letters*, **86**(1), 17-26. https://doi.org/10.1785/0220140104